Aircraft Power Generators: Hybrid Modeling and Simulation for Fault Detection

ASHRAF TANTAWY, Student Member, IEEE
XENOFON KOUTSOUKOS, Senior Member, IEEE
GAUTAM BISWAS, Senior Member, IEEE
Vanderbilt University

Integrated drive generators (IDGs) are the main source of electrical power for a number of critical systems in aircraft. Fast and accurate fault detection and isolation (FDI) are necessary components for safe and reliable operation of the IDG and the aircraft. IDGs are complex systems, and a majority of the existing FDI techniques for the electrical subsystem (brushless generator) are based on signal analysis and heuristic methods derived from experience. Model-based fault diagnosis techniques are hypothesized to be more general and powerful in designing detection and isolation schemes. However, building sufficiently accurate models of brushless generators is a difficult task. dq models have been developed for single generators, but these models are not suitable to represent the complete brushless generator either in normal or fault situations, where the generator may become unbalanced. In this paper, we develop a novel hybrid dynamical model for the complete brushless ac generator. We exploit the hybrid modeling capability to accurately model different rectifier diode faults and rotor winding faults, reported as the most severe brushless generator faults. We simulate the hybrid model for nominal and different faulty conditions, and develop fault signatures for different machine faults.

Manuscript received February 17, 2010; revised November 3 and December 27, 2010; released for publication January 21, 2011.

IEEE Log No. T-AES/48/1/943633.

Refereeing of this contribution was handled by W. Polivka.

This work was supported in part by NASA NRA NNX07AD12A.

A preliminary version of this work was presented at the International Conference on Prognostics and Health Management, PHM 2008.

Authors' address: Institute for Software Integrated Systems and the Department of Electrical Engineering and Computer Science, 1025 16th Ave. South, Vanderbilt University, Nashville, TN, 37235, E-mail: (ashraf.tantawy@vanderbilt.edu).

I. INTRODUCTION

The Integrated drive generator (IDG) is the primary source for electrical power in the aircraft. The system draws its power from the main aircraft engines and comprises two synchronous generators that operate in a brushless configuration. It also includes a number of other subsystems that convert the mechanical energy into electrical energy at a prespecified voltage and frequency. Since the machine operates in harsh environments, different components are subject to degradations and faults that can vary in terms of their critical effects on system behavior. For the electrical subsystem of the IDG, the most critical faults are winding faults and rectifier diode failures [4]. Fast and accurate fault detection and isolation (FDI) is a necessary component for the safe and reliable operation of the IDG, and, therefore, the aircraft.

The majority of existing techniques for FDI of synchronous generators are model free [5, 7, 20, 25]. Some of these techniques require the installation of additional hardware, e.g., search coils, yet this may not be possible for existing IDG installations. Other techniques assume special machine designs, e.g., the ability to measure circulating current in the main armature winding, or have access to measurements that are not available in brushless designs. Harmonic analysis has been proposed as an alternative technique to detect machine faults, but fault discrimination with harmonic analysis is a difficult task since different faults have a similar effect on the harmonics generated in the machine windings during faulty operations.

On the other hand, model-based diagnosis (MBD) techniques that utilize structural and analytic information captured in the system model provide a more general and powerful framework for designing FDI schemes [10, 12]. The distinguishing feature of MBD approach is the use of a system model that describes the laws which govern the behavior of the system for all possible inputs. Once a model is provided, the MBD engine should be able to detect system faults by comparing its input/output observations with the predicted behavior using the provided model. Furthermore, different models can be provided to the MBD engine for different faults, and the MBD would be able to diagnose the fault, by comparing the actual system behavior with the predicted behavior from different models [11]. An added benefit of MBD is that it provides methods for establishing the set of measurements required to discriminate among different fault types (i.e., the measurement selection problem [23]).

Despite the advantages of MBD, little work has been done in this area for brushless generators. One of the reasons is that constructing an appropriate model for the machine is challenging due to the multiple phenomena that need to be captured by the

model. In addition, the resulting model is, in general, a complex, nonlinear, and time-varying model that is hard to analyze. Despite these challenges, there are some practical considerations and reasonable approximations that, if taken into account while building the model, result in a simpler model, yet with sufficient accuracy to capture the machine behavior aspects. For example, current machine implementations allow continuous operation in the linear range of the magnetic curve, except for overload conditions. Therefore, unless it is desired to study the machine behavior during overload conditions, magnetic saturation could be neglected. Also, from a practical point of view, the mechanical subsystem that regulates the speed of rotation is robust to electrical subsystem fluctuations, due to sophisticated feedback control algorithms. Therefore, the mechanical subsystem could be decoupled from the electrical subsystem with minor loss of model accuracy. Similar approximations and practical considerations can result in system representations that are easier to analyze.

The first contribution of this paper is the development of a novel hybrid dynamical model for the complete brushless ac generator, based on phase domain representation. The key to model-based techniques is to build an accurate model for the system. The traditional approach for modeling ac synchronous generators is based on the dq model, where the well-known dq transformation is applied to the state variables (winding fluxes or currents) to convert the linear time-varying system to a linear time-invariant one in the dq frame of reference [1, 14]. To obtain a time-invariant system, the transformation assumes that symmetric conditions apply to the machine model. When faults occur in the system, or a nonlinear load is connected to the machine, the conditions of symmetry are violated for the IDG exciter generator with the rectifier circuit as a load. In this case, the dq transformation does not produce a time-invariant system, therefore, the advantages of applying the transformation are lost. In general, dq modeling is useful only for the analysis and simulation of the normal behavior of generators, where the normal operating range is sufficient for designing generator feedback controllers. However, if it is important to study and analyze a wide variety of machine configurations and transient phenomena (especially those caused by faults), then a phase domain behavior model (with no transformations) more accurately represents the resultant behavior, and, therefore, is more useful for FDI applications. Moreover, the phase domain representation has the advantage of handling the inherent asymmetries in the brushless design. With the goal of MBD, we focus on methods for systematically modeling and simulating a variety of nominal and faulty behaviors of the complete brushless generator.

In typical simulation studies, the focus is on the modeling of a single generator [22, 28]. The exciter generator and the rectifier circuit are represented by a constant dc voltage source. This approach is adequate for the fault-free exciter generator and rectifier circuits, but recent fault criticality analysis studies have shown that the highest priority failure modes are rotor field winding faults, rotating rectifier diode faults, and shaft bearing failures [4]. Therefore, to satisfy the need for more accurate models for FDI of the generators, we have to build models that accurately capture the exciter generator dynamics. Since the output of the exciter generator is connected to a rectifier circuit that contains switching elements, we adopt a hybrid modeling approach, where discrete and continuous dynamics are combined, to accurately model the complete brushless ac generator under normal and faulty conditions.

The second contribution of the paper is the accurate modeling of the IDG in the presence of different rectifier diode faults and winding faults, using the hybrid system modeling approach. For diode faults, a short circuit fault eventually leads to an open circuit condition, as the resultant over current burns the diode. Therefore, we only consider open circuit diode faults in this paper. Field winding faults could be either parametric or structural faults, where parametric faults are characterized by a change in the magnitude of one (or more) system model parameters, while structural faults change the system configuration and cannot be represented by a system parameter magnitude change alone. We focus our attention on parametric faults to simplify the exposition in this paper. However, the proposed model could be easily extended to include structural faults, by including the additional current loops in the model representation. We show that the proposed hybrid model can be effectively used to represent the brushless generator for the two fault types considered.

Our third contribution is the implementation and simulation of the hybrid system model, under normal and faulty conditions. This emphasizes the power of model-based methods to capture system dynamic behavior. Using the hybrid model, we develop fault signatures for rectifier diode faults and winding parametric faults. The fault signatures include nonmeasurable signals in addition to the measured terminal signals. The inclusion of nonmeasurable signals is unique to model-based FDI since it is possible to estimate the hidden states of the system, subject to the satisfaction of system observability conditions.

The work presented in this paper represents a generalization of our previous work where the model was developed for the exciter generator and rectifier only [29]. In addition to winding faults considered in [29], rectifier diode faults are thoroughly investigated in this paper. Different combinations of diode faults

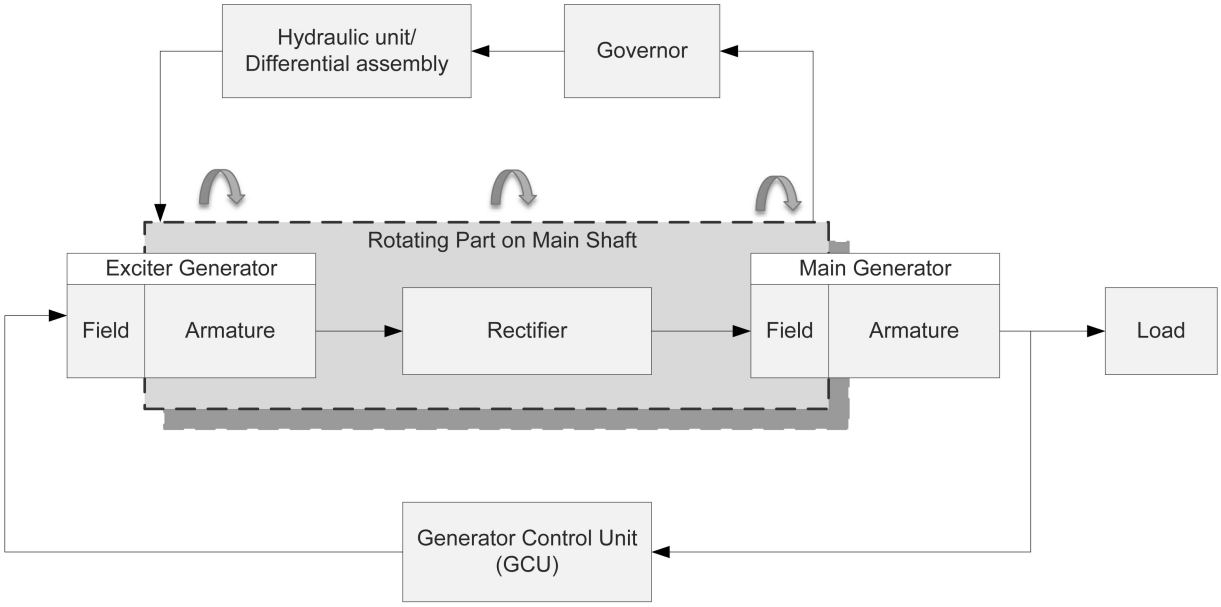

Fig. 1. IDG system block diagram. Electrical subsystem includes exciter generator, rectifier, and main generator with connected load. It is controlled by the GCU. The mechanical subsystem includes the governor and the differential assembly. System components enclosed in gray box rotate with main shaft, while remaining components are stationary, giving rise to brushless design.

are injected and simulated and a fault signature table is extracted from simulation results with guidelines for possible detection and diagnosis methods.

The rest of the paper is organized as follows. Section II describes the IDG block diagram, explaining different system components and their function. Section III presents a brief literature search for existing techniques of modeling and fault detection in synchronous generators. Section IV discusses our hybrid model for the brushless generator. Section V includes a discussion on modeling different types of field winding faults. Section VI presents a general framework to extend the generator model to include an arbitrary number of open-circuit diode faults. Section VII presents simulation results for normal and different faulty behaviors of the machine. Section VIII includes a discussion on modeling and simulation results, and Section IX concludes the work.

II. AIRCRAFT IDG

Fig. 1 illustrates the IDG system block diagram. The modeled generator operates in a 3-phase brushless configuration, with its drive end connected to a prime mover that is driven by the aircraft engine. The electrical subsystem is composed of four main components: the exciter generator, the rectifier, the main generator (with connected load), and the generator control unit (GCU). The exciter generator field current produces a magnetic field whose strength is proportional to the exciter current. The rotation of the prime mover in the magnetic field induces a 3-phase voltage in the exciter armature, which is rectified by the three-phase diode rectifier. The dc voltage current (with ripples) from the diode rectifier is then applied to the main generator field winding, which produces a 3-phase voltage in the main generator armature connected to the load. To keep the terminal voltage at (or close to) its operating value, the GCU calculates the rms value of the 3-phase voltages, compares it with a reference value, and regulates the field voltage of the exciter generator, using a predefined control algorithm. The exciter generator armature, rectifier, and the main generator field (enclosed in a gray dashed rectangular box) rotate with the main shaft that drives the entire brushless generator system, while the exciter field, the main generator armature, the GCU, and the load are stationary.

The mechanical subsystem is composed of the governor, which regulates the shaft speed by acting on a hydraulic unit/differential assembly. The differential unit adds or subtracts speed to drive the generator at a constant speed despite the variations of engine speed.

In this paper, we model the electrical subsystem including the exciter generator, rectifier, and the main generator with connected load. To simplify the presentation, we model the governor as a simple PI controller and assume ideal hydraulic/differential assembly, where the output of the PI controller represents the mechanical torque that is applied directly to the IDG.

III. RELATED WORK

The standard model used to represent a single synchronous ac generator is the dq model, that is based on Park's transformation [24]. Whereas the dq model is very useful to represent symmetric machine operations under balanced conditions, these

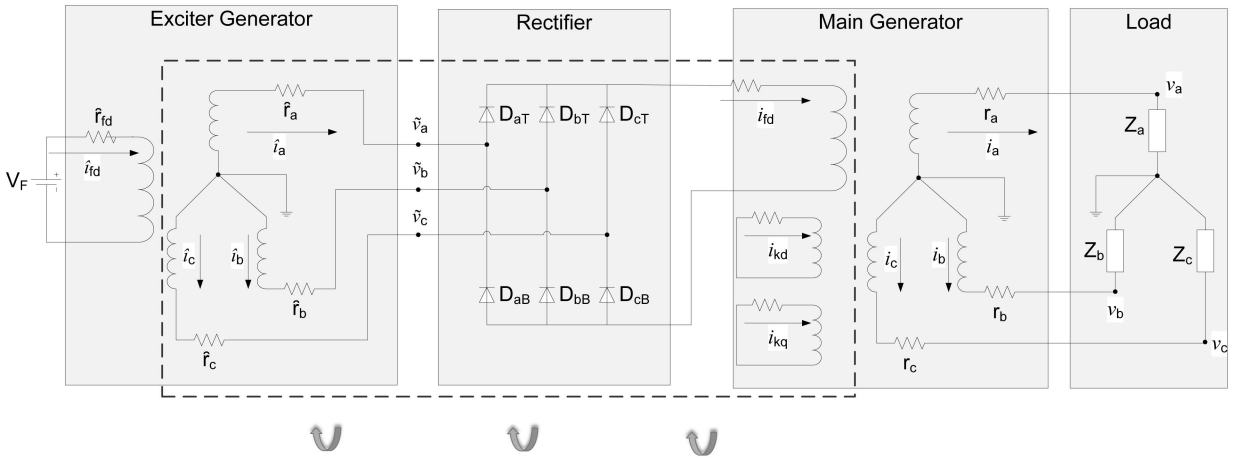

Fig. 2. Brushless ac generator electrical schematic diagram.

advantages are lost when analyzing unbalanced conditions, or asymmetrical faults [28]. For these cases, the abc modeling approach is more appropriate [14].

To model the complete brushless generator, both synchronous generators and the rectifier circuit have to be explicitly modeled. The rectifier is composed of switching elements (diodes) which introduce discrete dynamics into the overall system behavior. The traditional way of analyzing switching circuits relies on averaging or discretization techniques to make analysis of the circuit more tractable [26]. To accommodate behaviors caused by diode faults, we explicitly model the diode components of the complete brushless generator. This requires the adoption of a hybrid systems modeling approach [2].

Winding faults have received considerable attention in the literature, and different approaches have been proposed for winding fault detection. Specifically, the use of search coils to measure airgap flux asymmetry has been proposed to detect inter-turn faults [8]. This requires extra equipment that may be difficult to install in existing machines. For short circuit faults, one approach is to measure the circulating current in the main armature coils [27]. This approach is dependent on the generator design and cannot be applied in general. Another approach is the injection of voltage pulses in the rotor field winding and measuring the reflected signal [15]. This technique is clearly not applicable on brushless designs where the rotor field winding is not accessible. Harmonic analysis has been proposed to detect and isolate field and armature windings inter-turn faults as well as phase to ground faults [6, 7, 25]. However, harmonic signals depend on generator construction and excitation, and change with varying loads, making the discrimination between faults and load fluctuations a difficult task.

Artificial neural networks (ANNs) have been proposed to diagnose internal machine faults in [20]. The difficulty with using neural networks is that they require large, comprehensive data sets that capture different modes of operation of the machine and a number of fault conditions and magnitudes to effectively classify fault conditions. Different combinations of loads, faults, fault locations and magnitudes, and current signal values are required to generate the training data sets. Unless sufficient data is available to cover a majority of these conditions, the neural network classifier will be inaccurate and it may generate incorrect results [9].

Researchers have paid less attention to the detection of rectifier diode faults when compared with winding faults. Diode faults, although not representing an immediate risk on the generating system, may develop into a condition causing machine malfunction [4]. The traditional way to detect diode faults is through harmonic analysis of the exciter generator field current [19], or by calculating a simple ratio of the rms main generator current to the exciter generator field current. The use of search coils in the airgap has also been proposed in [17].

In this paper we motivate our model-based approach for fault detection, by extending our previous work in [29] to model the complete IDG system and to study diode fault behavior in addition to winding faults. We model the system in sufficient detail, and then develop fault signatures by understanding the physics of the failure events. Unlike existing work that relies on existing measurements or adds new equipment to measure additional signals, having a complete model for the system with faulty conditions allows the estimation of hidden states, and therefore, expands the set of signals that could be exploited for FDI.

IV. BRUSHLESS AC GENERATOR HYBRID MODEL

Fig. 2 illustrates the electrical schematic diagram for the brushless generator system (excluding the GCU). Each generator is represented by a set of magnetically coupled windings, namely the field winding (denoted by fd), the 3-phase output windings (denoted by a, b, and c), and the damper windings

TABLE I
Glossary of Model Variables

Variable	Description
i_x	Winding-x current, main generator
$\hat{i}_x$	Winding-x current, exciter generator
v_x	Winding-x voltage, main generator
$\hat{v}_x$	Winding-x voltage, exciter generator
λ_x	Winding-x flux linkage, main generator
$\hat{\lambda}_x$	Winding-x flux linkage, exciter generator
r_x	Winding-x resistance, main generator
$\hat{r}_x$	Winding-x resistance, exciter generator
ω	Electrical angular velocity
θ_r	Angular displacement
T_m	Mechanical input torque
P	Number of pole pairs of the main/exciter generators
J	Rotor inertia
D	Damping coefficient of the mechanical rotational system

(denoted by kq and kd). The damper windings are used only in the main generator. The rectifier circuit is represented by a 3-phase diode bridge circuit.

Table I lists a glossary of the state variables and resistance parameters used in the model, where subscript $x \in \{a,b,c,kq,fd,kd\}$ corresponds to a specific winding. To differentiate between the parameters and state variables for the exciter generator and the main generator, we use the $\hat{\cdot}$ notation, e.g. $\hat{r}_a$, for exciter generator variables. A complete glossary for model parameters is found in Tables III and IV.

We derive the mathematical model for the complete generating system by applying the Kirchoff's voltage law (KVL) equations to each winding, taking into account the magnetic coupling between the different windings. However, the rectifier circuit with its switching diodes creates multiple configurations (modes) for the system. Each mode of operation is defined by the combinations of forward and reverse-biased diodes in the rectifier, and the system behavior in each mode is defined by a set of differential equations.

We model diodes as ideal switches, acting as short circuit when forward-biased, and open circuit when reverse-biased. A detailed model for the rectifier that takes into account the conduction overlap phenomenon (arising from exciter generator inductances) would require 13 modes of operation; six modes for the classical conduction, six modes of overlap, and one discontinuous conduction mode [3]. In this paper, we ignore the conduction overlap phenomenon and model only the classical conduction modes to simplify the exposition. However, the reader should note that the impact of modeling the conduction overlap is the addition of extra modes in the hybrid model with the relevant dynamics. Therefore, the results presented here would still be applicable with a straightforward extension of the model. Table II lists the six classical modes of operation with their relevant terminal voltage

TABLE II
Generator Hybrid Model Modes of Operation

Mode	Exciter Terminal Voltage Condition	Forward-Biased Diodes
AB	$\hat{v}_a > \hat{v}_c > \hat{v}_b$	D_{aT} and D_{bB}
AC	$\hat{v}_a > \hat{v}_b > \hat{v}_c$	D_{aT} and D_{cB}
BC	$\hat{v}_b > \hat{v}_a > \hat{v}_c$	D_{bT} and D_{cB}
BA	$\hat{v}_b > \hat{v}_c > \hat{v}_a$	D_{bT} and D_{aB}
CA	$\hat{v}_c > \hat{v}_b > \hat{v}_a$	D_{cT} and D_{aB}
CB	$\hat{v}_c > \hat{v}_a > \hat{v}_b$	D_{cT} and D_{bB}

conditions, and the forward-biased diodes (all remaining diodes are reverse-biased).

Fig. 3 shows the corresponding system automaton with the six discrete modes and the guard conditions expressed in terms of exciter generator terminal voltages. The ignored modes of overlap would fit between every pair of the classical modes, with obvious guard conditions. As an example, an additional mode between modes AB and AC would be needed to represent the overlapping period where diodes D_{aT}, D_{bB}, and D_{cB} are simultaneously forward-biased. For every discrete mode, the system evolves according to its continuous dynamics. For brevity, we present the mathematical model for mode AB only, but the dynamics of the other discrete states can be derived in a similar way.

The electrical schematic diagram for mode AB is illustrated in Fig. 3. Inside the dashed box, windings a and b of the exciter generator and winding fd of the main generator are connected together, while winding c of the exciter generator is floating. Applying KVL, we get the following set of equations:

$$\dot{\lambda}_a = r_a i_a + v_a \tag{1}$$

$$\dot{\lambda}_b = r_b i_b + v_b \tag{2}$$

$$\dot{\lambda}_c = r_c i_c + v_c \tag{3}$$

$$\dot{\lambda}_{kq} = -r_{kq} i_{kq} \tag{4}$$

$$\dot{\hat{i}}_a - \dot{i}_{fd} = 0 \tag{5}$$

$$\dot{\lambda}_{kd} = -r_{kd} i_{kd} \tag{6}$$

$$\dot{\hat{\lambda}}_a - \dot{\hat{\lambda}}_b - \dot{\lambda}_{fd} = (\hat{r}_a + \hat{r}_b + r_{fd})\hat{i}_a \tag{7}$$

$$\dot{\hat{i}}_a + \dot{\hat{i}}_b = 0 \tag{8}$$

$$\dot{\hat{i}}_c = 0 \tag{9}$$

$$\dot{\hat{\lambda}}_{fd} = -\hat{r}_{fd}\hat{i}_{fd} + V_F \tag{10}$$

$$\dot{\omega} = \frac{P}{2J}(T_m - T_e - \hat{T}_e - D\omega) \tag{11}$$

$$\dot{\theta}_r = w. \tag{12}$$

T_e and $\hat{T}_e$ denote the electric (load) torque of the main and exciter generators, respectively, and are given

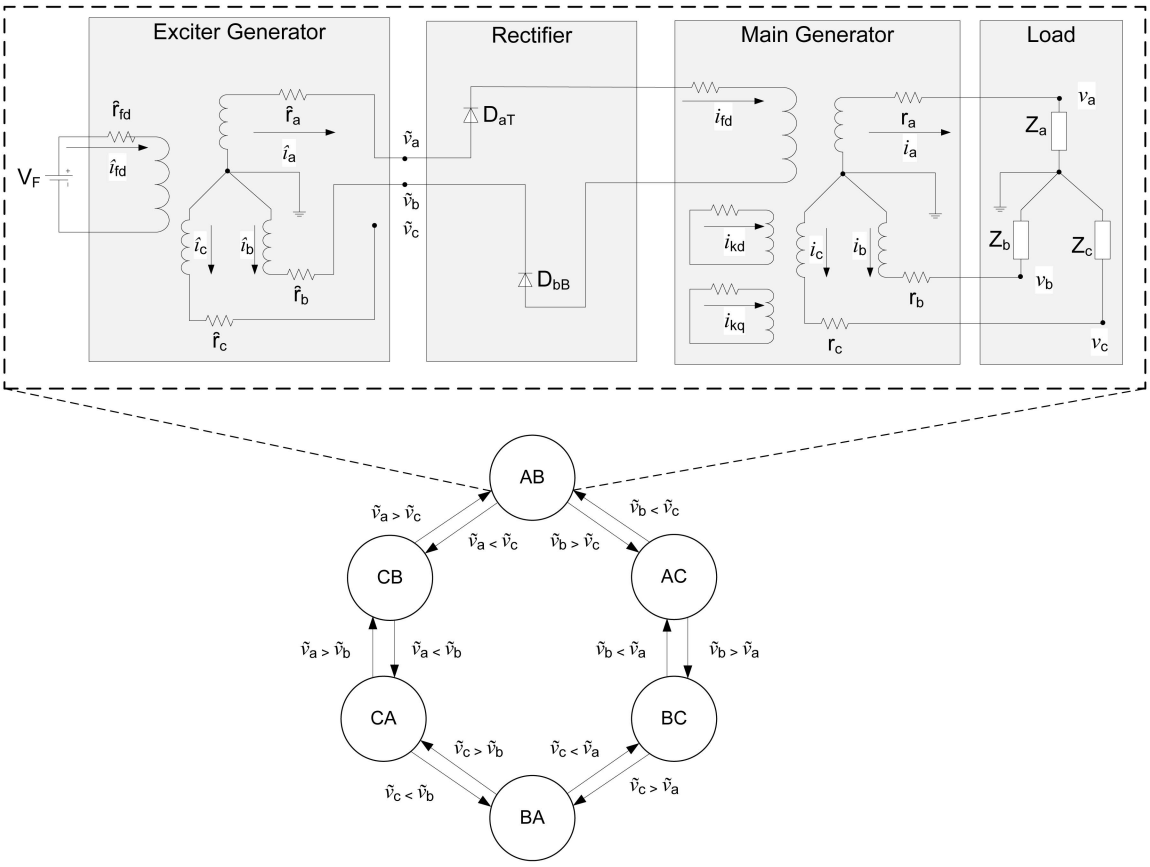

Fig. 3. Brushless generator system automaton. Dashed box shows electrical schematic diagram when system is in mode *AB*, where windings a and b of exciter generator, and winding fd of main generator are connected together, while winding c of exciter generator is floating.

by [14]:

$$\begin{aligned}T_e = {} & \frac{P(L_{mq}-L_{md})}{6}[i_a^2 - 0.5(i_b+i_c)^2 - i_a(i_b+i_c)]\sin(2\theta_r) \\ & + \frac{PL_{md}}{3}\left(\frac{N_{fd}}{N_s}i_{fd} + \frac{N_{kd}}{N_s}i_{kd}\right)[i_a - 0.5i_b - 0.5i_c]\cos(\theta_r) \\ & + \frac{\sqrt{3}P(L_{mq}-L_{md})}{8}(i_b^2 + i_c^2 - 2i_ai_b + 2i_ai_c)\cos(2\theta_r) \\ & + \frac{P(L_{mq}-L_{md})}{2}i_bi_c\sin(2\theta_r) + \frac{PL_{md}}{2\sqrt{3}}[i_b - i_c]\sin(\theta_r) \\ & - \frac{N_{kq}P}{3N_s}L_{mq}i_{kq}[i_a - 0.5i_b - 0.5i_c]\sin(\theta_r) \\ & + \frac{N_{kq}P}{2\sqrt{3}N_s}L_{mq}i_{kq}[i_b - i_c]\cos(\theta_r) \end{aligned} \tag{13}$$

$$\begin{aligned}\hat{T}_e = {} & \frac{P(\hat{L}_{mq}-\hat{L}_{md})}{6}[\hat{i}_a^2 - 0.5(\hat{i}_b^2+\hat{i}_c)^2 - \hat{i}_a(\hat{i}_b+\hat{i}_c)]\sin(2\theta_r) \\ & + \frac{\sqrt{3}P(\hat{L}_{mq}-\hat{L}_{md})}{8}(\hat{i}_b^2 + \hat{i}_c^2 - 2\hat{i}_a\hat{i}_b + 2\hat{i}_a\hat{i}_c)\cos(2\theta_r) \\ & + \frac{\hat{N}_{fd}P}{2\sqrt{3}\hat{N}_s}[\hat{i}_b - \hat{i}_c]\sin(\theta_r) + \frac{P(\hat{L}_{mq}-\hat{L}_{md})}{2}\hat{i}_b\hat{i}_c\sin(2\theta_r) \\ & + \frac{\hat{N}_{fd}P}{3\hat{N}_s}\hat{L}_{md}\hat{i}_{fd}[\hat{i}_a - 0.5\hat{i}_b - 0.5\hat{i}_c]\cos(\theta_r). \end{aligned} \tag{14}$$

There are 12 state variables, representing the currents in the different windings, in addition to the angular displacement θ_r, and angular velocity ω. From (5), (8), and (9), we have four dependent currents, which reduces the state variables to nine. However, we use the twelve state variables to keep the model representation consistent between the different modes, and also to facilitate model implementation.

We define the following vectors:

$$\boldsymbol{\lambda} = [\lambda_a \quad \lambda_b \quad \lambda_c \quad \lambda_{kq} \quad \lambda_{fd} \quad \lambda_{kd}]^T$$

$$\mathbf{i} = [i_a \quad i_b \quad i_c \quad i_{kq} \quad i_{fd} \quad i_{kd}]^T$$

$$\hat{\boldsymbol{\lambda}} = [\hat{\lambda}_a \quad \hat{\lambda}_b \quad \hat{\lambda}_c \quad \hat{\lambda}_{fd}]^T$$

$$\hat{\mathbf{i}} = [\hat{i}_a \quad \hat{i}_b \quad \hat{i}_c \quad \hat{i}_{fd}]^T$$

$$\begin{aligned}\mathbf{R} = [r_a \quad r_b \quad r_c \quad -r_{kq} \quad 0 \quad -r_{kd} \quad \hat{r}_a \\ + \hat{r}_b + r_{fd} \quad 0 \quad 0 \quad -\hat{r}_{fd}]\end{aligned}$$

$$\mathbf{u} = [v_a \quad v_b \quad v_c \quad 0 \quad 0 \quad 0 \quad 0 \quad 0 \quad 0 \quad V_F]^T.$$

We have the following λ-i relationship for the main generator:

$$\boldsymbol{\lambda} = \mathbf{L}\mathbf{i} \quad \Rightarrow \quad \dot{\boldsymbol{\lambda}} = \mathbf{L}\dot{\mathbf{i}} + \dot{\mathbf{L}}\mathbf{i} \tag{15}$$

and for the exciter generator:

$$\hat{\boldsymbol{\lambda}} = \hat{\mathbf{L}}\hat{\mathbf{i}} \quad \Rightarrow \quad \dot{\hat{\boldsymbol{\lambda}}} = \hat{\mathbf{L}}\dot{\hat{\mathbf{i}}} + \dot{\hat{\mathbf{L}}}\hat{\mathbf{i}} \tag{16}$$

where $\mathbf{L}$ and $\hat{\mathbf{L}}$ are the inductance matrices for the main and exciter generators, respectively. The matrices are time varying, depending on the angular displacement θ_r, and their expressions are given in the Appendix. Combining (1)–(16) together, and using the notation $\mathbf{L}_2$ to designate row 2 of matrix $\mathbf{L}$, and $\mathbf{1}_{nm}^{i_1 j_1, i_2 j_2, \cdots}$ to designate an $n \times m$ matrix with all zero elements except elements $(i_1, j_1), (i_2, j_2), \ldots$, we get

$$\mathbf{M}\begin{bmatrix} \dot{\mathbf{i}} \\ \dot{\hat{\mathbf{i}}} \end{bmatrix} = (\mathbf{N} + \mathbf{R})\begin{bmatrix} \mathbf{i} \\ \hat{\mathbf{i}} \end{bmatrix} + \mathbf{u}$$

where

$$\mathbf{M} = \begin{bmatrix} \mathbf{L}_1 & \mathbf{0} \\ \mathbf{L}_2 & \mathbf{0} \\ \mathbf{L}_3 & \mathbf{0} \\ \mathbf{L}_4 & \mathbf{0} \\ -\mathbf{1}_{16}^{15} & \mathbf{1}_{14}^{11} \\ \mathbf{L}_6 & \mathbf{0} \\ -\mathbf{L}_5 & \hat{\mathbf{L}}_1 - \hat{\mathbf{L}}_2 \\ \mathbf{0} & \mathbf{1}_{14}^{11,12} \\ \mathbf{0} & \mathbf{1}_{14}^{13} \\ \mathbf{0} & \hat{\mathbf{L}}_4 \end{bmatrix}, \quad \mathbf{N} = \begin{bmatrix} -\dot{\mathbf{L}}_1 & \mathbf{0} \\ -\dot{\mathbf{L}}_2 & \mathbf{0} \\ -\dot{\mathbf{L}}_3 & \mathbf{0} \\ -\dot{\mathbf{L}}_4 & \mathbf{0} \\ \mathbf{0} & \mathbf{0} \\ -\dot{\mathbf{L}}_6 & \mathbf{0} \\ \dot{\mathbf{L}}_5 & \dot{\hat{\mathbf{L}}}_2 - \dot{\hat{\mathbf{L}}}_1 \\ \mathbf{0} & \mathbf{0} \\ \mathbf{0} & \mathbf{0} \\ \mathbf{0} & -\dot{\hat{\mathbf{L}}}_4 \end{bmatrix} \tag{17}$$

where $\mathbf{0}$ and $\mathbf{1}$ are column vectors of 0 and 1, respectively, with appropriate dimensions. The state-space model for the complete system is then given by

$$\begin{aligned} \begin{bmatrix} \dot{\mathbf{i}} \\ \dot{\hat{\mathbf{i}}} \end{bmatrix} &= \mathbf{M}^{-1}(\mathbf{N} + \mathbf{R})\begin{bmatrix} \mathbf{i} \\ \hat{\mathbf{i}} \end{bmatrix} + \mathbf{M}^{-1}\mathbf{u} \\ \dot{\omega} &= \frac{P}{2J}(T_m - T_e - \hat{T}_e - D\omega) \\ \dot{\theta}_r &= w. \end{aligned} \tag{18}$$

This represents a nonlinear, time-varying system. It should be highlighted that the state-space model given by (18) is not a complete system description, since the main generator terminal voltages have to be defined in terms of the state variables, i.e., the winding currents. For example, if we assume a resistive load R_a, R_b, R_c, then the complete state-space model is still given by (18) with the following definition for $\mathbf{R}$ and $\mathbf{u}$:

$$\begin{aligned} \mathbf{R} = \operatorname{diag}(&R_a + r_a, R_b + r_b, R_c + r_c, -r_{kq}, 0, \\ &-r_{kd}, \hat{r}_a + \hat{r}_b + r_{fd}, 0, 0, -\hat{r}_{fd}) \end{aligned} \tag{19}$$

$$\mathbf{u} = [0 \quad 0 \quad 0 \quad 0 \quad 0 \quad 0 \quad 0 \quad 0 \quad 0 \quad V_F]^T. \tag{20}$$

The model presented in this section is implemented in Matlab/Simulink®, and the nominal behavior of the machine is discussed in Section VIIA. The nominal behavior is also summarized in Fig. 7.

V. MODELING MAIN FIELD WINDING FAULTS

Generator winding faults can be classified into one of two main categories: parametric faults and structural faults [29]. Parametric faults are characterized by a change in the magnitude of one or more system model parameters. These faults do not affect the structure of the system, and, therefore, the system model is still a valid representation for the actual system. Structural faults change the system configuration and cannot be captured by a magnitude change in the system parameters. The system model under these faults is no longer valid, and a new model representing the new configuration is necessary to generate the system behavior.

Parametric faults can be further classified into abrupt and incipient faults, where abrupt faults describe a sudden change in system parameters, while incipient faults describe a degradation that evolves continuously with time. An example of an abrupt fault is the sudden increase of a winding resistance, or the sudden decrease in the number of windings, due to shorted turns. An example of an incipient fault is the gradual increase of winding resistance due to overheating of the rotating part.

Parametric faults can be represented easily using the hybrid model presented in Section IV. The structure of the model remains the same, including the discrete modes and the continuous dynamics equations, although the continuous dynamics for every discrete mode will be different depending on the new parameter values.

Structural faults can be classified into external and internal faults. External faults are the ones that happen outside the machine terminals, and although they do not change the structure of the machine, the overall system model changes. An example is a phase-to-phase short circuit fault. Internal faults are intrinsic to the machine itself (within the machine boundary). An example of an internal fault that changes the structure of the system is a phase-to-ground short circuit. The short circuit from the winding to the ground creates a new loop with voltage equal to 0 [21]. The machine with the short circuit fault could be modeled in a similar way to the one presented in Section IV, by including the new loop. The number of discrete modes will remain the same, since it is related to the rectifier circuit, but the continuous dynamics inside every discrete mode will be different. The situation becomes more complex

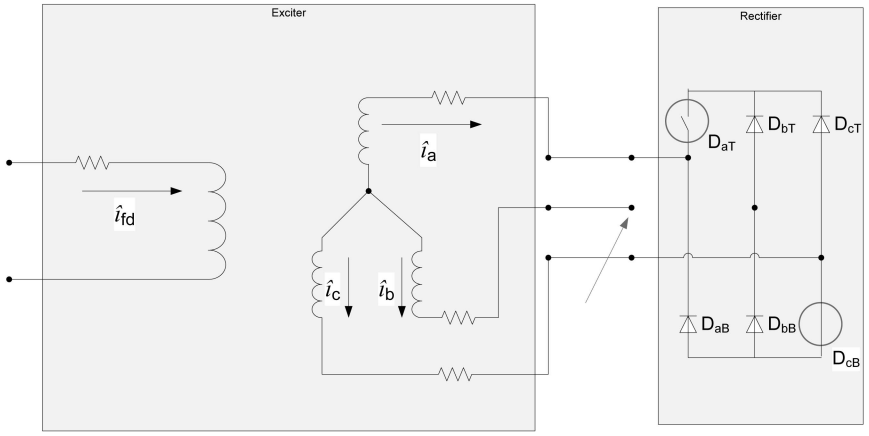

Fig. 4. Brushless generator rectifier faults. Diode D_{aT} fails open, diode D_{cB} fails closed, while phase b is disconnected from rectifier circuit.

when there is a dual fault from two phases to the ground.

Field winding faults generally evolve over time, and structural faults are usually caused by persistent, small, parametric faults. For example, a small number of shorted turns may cause overheating in the magnetic core of the generator, which after a period of time causes structural winding to ground faults. Therefore, we consider only parametric faults for the field winding. As pointed out before, structural faults could be simulated by extending the hybrid model, with the added complexity represented by the increased system order.

An example of a single parametric fault, an abrupt increase in the main generator field winding resistance r_{fd}, is simulated. The results are discussed in Section VIIC, and the behavior is summarized in Fig. 10.

VI. MODELING RECTIFIER DIODE FAULTS

In this section we exploit the hybrid model presented in Section IV to model the brushless generator with different combinations of diode faults. We first identify rectifier circuit fault types, then we present an algorithm to identify the discrete dynamics for the system with any combination of faulty diodes. We give examples for different faults to explain the algorithm implementation.

Studying the rectifier circuit shows that faults could occur in either the diodes or the cables connecting the three-phase output of the exciter generator to the rectifier circuit. Diodes fail in one of two ways: failed open or failed short. In practice, shorted diodes often overheat, and burn out causing open circuits. Therefore, we address open circuit diode faults in this paper. Cable faults are diverse, and we restrict ourselves in this study to discrete cable faults, where one of the 3 phases of the exciter generator is no longer connected to the rectifier circuit. Fig. 4 illustrates the three types of faults, where diode D_{aT} is open, diode D_{cB} is shorted, and phase b is disconnected from the rectifier circuit. It can be easily shown that the loss of one phase is equivalent to two diodes suffering open circuit failures in the vertical branch of the rectifier connected to the faulty phase.

The six discrete modes presented in Table II represent the maximum set of modes that the system can be in for any normal or faulty behavior. In other words, the system with rectifier diode faults can be represented with a subset of the set composed of the six discrete modes of the system. An additional OFF mode may be needed for the case of multiple diode faults, representing the rectifier circuit when in off mode (not conducting, i.e., the exciter and main generators are decoupled). Algorithm 1 provides a formal procedure to specify valid system modes and to define system behavior. The algorithm is general and could be applied to single and multiple diode faults, as well as phase faults.

We describe some terminology that is used in Algorithm 1. We designate the set of diodes for the rectifier circuit by $D = \{D_{ij},\ i \in P = \{a,b,c\},\ j \in \{T,B\}\}$, where i represents the connected phase and j represents the position of the diode (top or bottom). The set of faulty diodes is denoted by $F \subset D$. $\Omega = \{AB,AC,BC,BA,CA,CB\}$ is the set of the discrete modes for the brushless hybrid system, and $\Omega_f = \Omega \cup \{OFF\}$ is the set of the discrete modes for the brushless hybrid system, covering both normal and faulty system behavior. The set of valid discrete system modes after a diode fault has occurred is denoted by $M \subset \Omega_f$, and the set of excluded system modes is denoted by $\bar{M} = \Omega_f - M$. Finally, $g : \Omega \mapsto \Omega_f$ is a function mapping defining the replacement for every excluded system mode, i.e., it defines the discrete mode the system resides in during the time period originally allocated to the excluded mode.

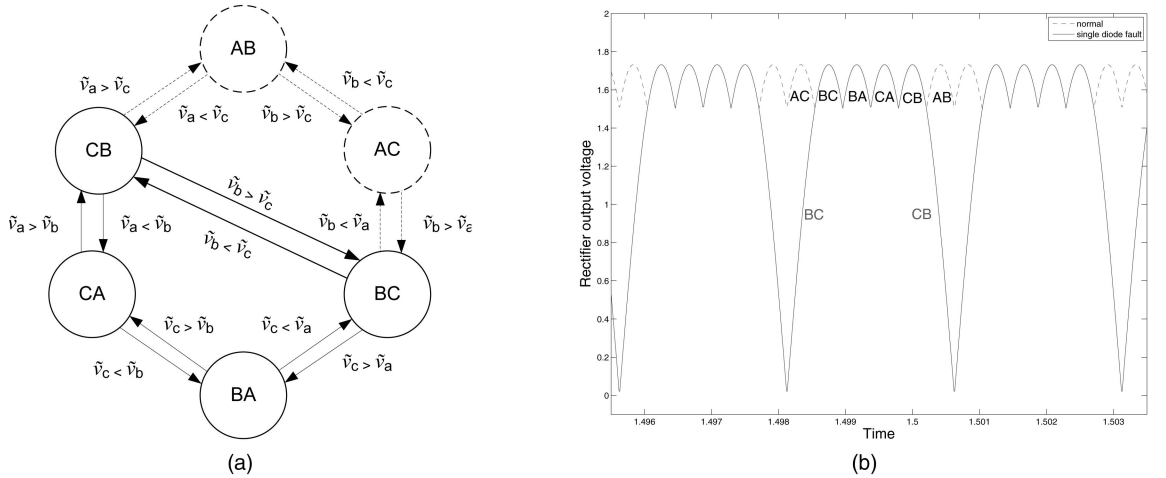

Fig. 5. System automaton and rectifier output voltage for single diode fault. (a) System automaton with rectifier diode D_{aT} open circuit fault. Modes AB and AC are no longer valid system modes, and system jumps from mode CB directly to mode BC. Time for mode AB is spent in mode CB, and time for mode AC is spent in mode BC. (b) Rectifier output voltage with single diode fault, for diode D_{aT}. Labels indicate active system mode during every time period. Dashed curve refers to normal output voltage, while solid curve represents output with diode fault. Modes AC and AB are not valid system modes with D_{aT} fault, and system moves from mode CB to mode BC directly, causing return to zero for rectifier output voltage.

ALGORITHM 1 *Specifying valid system modes and system behavior with rectifier diode faults*

Input: F
Output: $M, g(.)$
{*define excluded system modes*}
for $k \in F$ **do**
  if $j = T$ **then**
    $\bar{M}_k = \{\bar{i}i : \bar{i} = P - i\}$
  else
    $\bar{M}_k = \{\bar{i}i : \bar{i} = P - i\}$
  end if
end for
$\bar{M} = \cup_{k \in F} \bar{M}_k, M = \Omega - \bar{M}$ {*set of valid system modes*}
{*define system behavior and whether OFF state is required*}
for $m = p_1 p_2 \in \Omega$ **do**
  if $m \in M$ **then**
    $\bar{p} = P - \{p_1, p_2\}$
    $m_1 = p_1\bar{p}, m_2 = \{\bar{p}p_2\}$ {m_1 *and* m_2 *cannot be valid system modes simultaneously, otherwise* m *will not be an excluded mode.*}
    if $m_1 \in M$ **then**
      $g(m) = m_1$
    else if $m_2 \in M$ **then**
      $g(m) = m_2$
    else
      $g(m) = OFF$
      $M = M \cup \{OFF\}$
    end if
  else
    $g(m) = m$
  end if
end for
return $M, g(.)$

In the following we give examples for single, dual diode, and phase faults. Examples refer to Fig. 2 for illustration purposes.

EXAMPLE 1 (Single Diode Fault) Assume diode D_{aT} failed in an open circuit position. Following Algorithm 1 with $F = \{D_{aT}\}$:

$$\bar{M}_{aT} = \{AB, AC\}$$

$$\bar{M} = \bar{M}_{aT} = \{AB, AC\}, \quad M = \{BA, CA, CB, BC\}$$

$$m = AB \quad m_1 = AC \text{ (excluded)} \quad m_2 = CB \text{ (valid)}$$

$$\Rightarrow g(AB) = CB \quad \text{AB time spent in CB}$$

$$m = AC \quad m_1 = AB \text{ (excluded)} \quad m_2 = BC \text{ (valid)}$$

$$\Rightarrow g(AC) = BC \quad \text{AC time spent in BC}$$

$$M = \{BA, CA, CB, BC\}$$

$$g(\Omega) = \{CB, BC, BC, BA, CA, CB\}.$$

Fig. 5(a) illustrates the system automaton under this new condition, with excluded modes and transitions marked with dashed lines. Fig. 5(b) shows the rectifier circuit output voltage (main generator field excitation) with D_{aT} diode fault, as compared with the normal output. The system spends the time of mode AB in mode CB, and the time for mode AC in mode BC. Also, since the rectifier output voltage is the difference between the connected terminal voltages v_a, v_b, and v_c (according to the active mode), the transition condition from mode CB to mode BC shows that the rectifier output voltage has to return to zero every complete cycle through system modes.

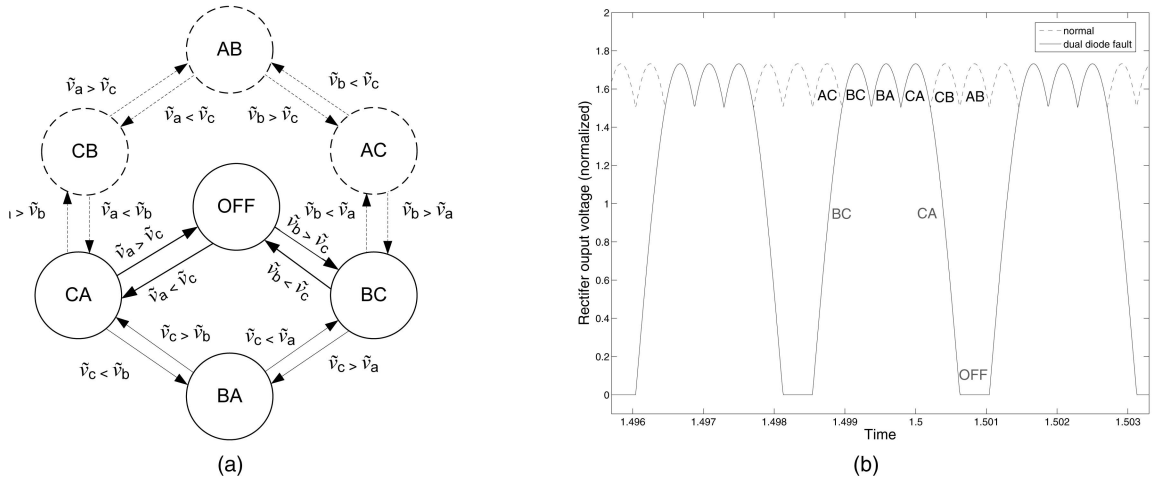

Fig. 6. System automaton and rectifier output voltage for dual diode fault. (a) System automaton with rectifier diodes D_{aT} and D_{bB} open circuit fault. Modes CB, AB, and AC are no longer valid system modes. Additional OFF mode is required, representing the case when rectifier circuit is not conducting, hence exciter and main generators are decoupled. Time for mode CB is allocated to CA, time for mode AC is allocated to BC, time for mode AB is allocated to OFF mode. (b) Rectifier output voltage with dual diode fault, for diode D_{aT} and D_{bB}. Labels indicate active system mode during every time period. Dashed curve refers to normal output voltage, while solid curve represents output with diode fault. Modes AC, CB, and AB are not valid system modes, and time for mode AB is allocated to OFF mode, representing no conduction for rectifier circuit.

If, on the other hand, diode D_{aB} fails in an open circuit position, then the same argument leads to the exclusion of modes BA and CA. Other single diode failures can be analyzed in a similar way.

EXAMPLE 2 (Dual Diode Fault) Assume diodes D_{aT} and D_{bB} failed in an open circuit position, then $F = \{D_{aT}, D_{bB}\}$:

$$\bar{M}_{aT} = \{AB, AC\}$$

$$\bar{M}_{bB} = \{AB, CB\}$$

$$\bar{M} = \bar{M}_{aT} \cup \bar{M}_{bB} = \{AB, AC, CB\}, \quad M = \{BA, BC, CA\}$$

$$m = AB \quad m_1 = AC \text{ (excluded)} \quad m_2 = CB \text{ (excluded)}$$

$$\Rightarrow g(AB) = OFF \quad \text{AB time spent in OFF state}$$

$$M = \{BA, BC, CA, OFF\}$$

$$m = AC \quad m_1 = AB \text{ (excluded)} \quad m_2 = BC \text{ (valid)}$$

$$\Rightarrow g(AC) = BC \quad \text{AC time spent in BC}$$

$$m = CB \quad m_1 = CA \text{ (valid)} \quad m_2 = AB \text{ (excluded)}$$

$$\Rightarrow g(CB) = CA \quad \text{CB time spent in CA}$$

$$M = \{BA, BC, CA, OFF\}$$

$$g(\Omega) = \{OFF, BC, BC, BA, CA, CA, OFF\}.$$

Fig. 6(a) illustrates the resulting system automaton. The system spends the time of mode CB in mode CA, the time of mode AB in mode OFF, and the time of mode AC in mode BC. This gives rise to the rectifier circuit output voltage in Fig. 6(b).

For phase faults, a discrete phase fault (losing one phase connection to the rectifier) is equivalent to two diode faults in the vertical branch connected to the phase. In this case, every phase loss results in an exclusion of four system modes, since every diode results in the exclusion of two modes, and the two diodes, being in one branch, do not have any common modes. Moreover, it can be easily shown that it is always true that there is a valid mode for the system when the transition condition to an excluded mode is satisfied. Therefore, OFF mode is not a valid system mode for phase faults. Phase faults can be modeled in a similar way to Examples 1 and 2.

The two types of faults presented in Examples 1 and 2 are simulated in this paper. The results are discussed in Section VIIB, and the behavior is summarized in Figs. 8 and 9, respectively.

VII. SIMULATION RESULTS

The complete mathematical model for the brushless generator, presented in Section IV, is implemented in Matlab/Simulink® [18], to generate behaviors under nominal and faulty conditions. A 400 Hz brushless generator, with the equivalent set of parameter values (in SI units) shown in Table III, is used for simulation. These parameters are in dq domain, and transformed to the phase-domain values using the equations shown in Table IV. The transformation is not unique since more than one ratio of the windings may result in the same set of parameter values in the phase domain. The parameter values are used for both the main and exciter generators. Primed parameters are field variables referred to the armature windings.

A. Nominal Behavior

The system is simulated with no faults to setup the reference signals for comparison purposes, when

TABLE III
dq Model Parameters

Parameter	Description	Value
L_{ls}	Leakage inductance, stator winding	0.004527 H
L_{md}	Magnetizing inductance, d winding	0.1086 H
L_{mq}	Magnetizing inductance, q winding	0.05175 H
$\acute{L}_{lkq}$	Leakage inductance, kq winding (referred)	0.01015 H
$\acute{L}_{lfd}$	Leakage inductance, fd winding (referred)	0.01132 H
$\acute{L}_{lkd}$	Leakage inductance, kd winding (referred)	0.007334 H
r_a	resistance, stator winding a	1.62 Ω
r_b	resistance, stator winding b	1.62 Ω
r_c	resistance, stator winding c	1.62 Ω
$\acute{r}_{kq}$	resistance, kq winding	4.772 Ω
$\acute{r}_{fd}$	resistance, fd winding	0.6 kΩ
$\acute{r}_{kd}$	resistance, kd winding	3.142 Ω
N_s	Number of turns, stator winding	100
N_{fd}	Number of turns, fd winding	100
N_{kq}	Number of turns, kq winding	100
N_{kd}	Number of turns, kd winding	100
D	Damping coefficient	0.009 kg.m^2.s^{-1}
J	Moment of inertia	0.0923 kg.m^2

TABLE IV
Phase-Domain Model Parameters Calculation

Parameter	Description	Expression
L_A	Machine geometrical parameter	$\frac{Lmd + Lmq}{3}$
L_B	Machine geometrical parameter	$\frac{Lmd - Lmq}{3}$
L_{lkq}	Leakage inductance, kq winding	$\left(\frac{2}{3}\right)\left(\frac{N_{kq}}{N_s}\right)^2 \acute{L}_{lkq}$
L_{mkq}	Magnetizing inductance, kq winding	$\left(\frac{2}{3}\right)\left(\frac{N_{kq}}{N_s}\right)^2 L_{mq}$
L_{lfd}	Leakage inductance, fd winding	$\left(\frac{2}{3}\right)\left(\frac{N_{fd}}{N_s}\right)^2 \acute{L}_{lfd}$
L_{lkd}	Leakage inductance, kd winding	$\left(\frac{2}{3}\right)\left(\frac{N_{kd}}{N_s}\right)^2 \acute{L}_{lkd}$
L_{skq}	Mutual inductance, stator-kq windings	$\left(\frac{2}{3}\right)\left(\frac{N_{kq}}{N_s}\right) L_{mq}$
L_{sfd}	Mutual inductance, stator-fd windings	$\left(\frac{2}{3}\right)\left(\frac{N_{fd}}{N_s}\right) L_{md}$
L_{skd}	Mutual inductance, stator-kd windings	$\left(\frac{2}{3}\right)\left(\frac{N_{kd}}{N_s}\right) L_{md}$
L_{fdkd}	Mutual inductance, fd-kd windings	$\left(\frac{N_{fd}}{N_{kd}}\right) L_{mkd}$
r_{kq}	Resistance, kq winding	$\left(\frac{2}{3}\right)\left(\frac{N_{kq}}{N_s}\right)^2 \acute{r}_{kq}$
r_{fd}	Resistance, fd winding	$\left(\frac{2}{3}\right)\left(\frac{N_{fd}}{N_s}\right)^2 \acute{r}_{fd}$
r_{kd}	Resistance, kd winding	$\left(\frac{2}{3}\right)\left(\frac{N_{kd}}{N_s}\right)^2 \acute{r}_{kd}$

studying system behavior with faults. The following signals are observed (Fig. 7):

Exciter generator winding currents: according to system dynamics description in Section IV, every phase current $\hat{i}_a$, $\hat{i}_b$, $\hat{i}_c$ is on for the duration of two modes (1/3 the generator output period ≈ 0.83 ms), off for 1/6 of the period, on (with opposite sign) for 1/3 of the period, and off for 1/6 of the period. The field current is steady with superimposed small magnitude oscillations.

Rectifier output voltage: the voltage is a typical output from a 3-phase rectifier, with average dc voltage and superimposed ripples.

Main generator winding currents: phase currents represent the nominal 3-phase sinusoidal output from the generator. Damper winding currents are equal to zero during steady state, with very small ripples. The field winding current signal exhibits the same behavior of its accompanying rectifier output voltage.

B. Diode Fault Injection

Single and dual diode faults are simulated. Diode designations are with reference to Fig. 2.

1) *Single Diode Fault*: The system is simulated with an open circuit fault in diode D_{aT}, injected at time $t = 0.5$ s. According to Section VI, this results in the discrete mode set $\{CB, BC, BA, CA\}$, and the automaton in Fig. 5(a). The following signals are observed (Fig. 8).

Exciter generator winding currents: because of excluded modes, $\hat{i}_a \leq 0$. $\hat{i}_b$ and $\hat{i}_c$ exhibit similar behavior to their nominal waveform, except that the transition from positive to negative half cycle for $\hat{i}_b$ is smooth with no abrupt return to zero as in the nominal case. The same is applied to $\hat{i}_c$ when switching from negative to positive half cycles. This can be easily explained by following the system automaton in Fig. 5(a). The exciter field winding current undergoes periodic oscillations with the same waveform as the rectifier output voltage, except that the waveform does not return to zero, but to a value that is > 0 and smaller than its steady state value.

Rectifier output voltage: the voltage returns to zero during modes AB and AC, as explained in Section VI. The signal does not match Fig. 5(b) as the 3-phase output from the exciter generator is not pure sinusoidal with rectifier diode faults.

Main generator winding currents: the 3-phase currents undergo distortion, which may be detected by harmonic analysis. The field winding signal behavior is very similar to the output voltage. An interesting behavior for damper winding currents is noted, since these currents are almost equal to zero in normal operation. With diodes fault, both currents undergo out-of-phase spikes at the time of fault injection,

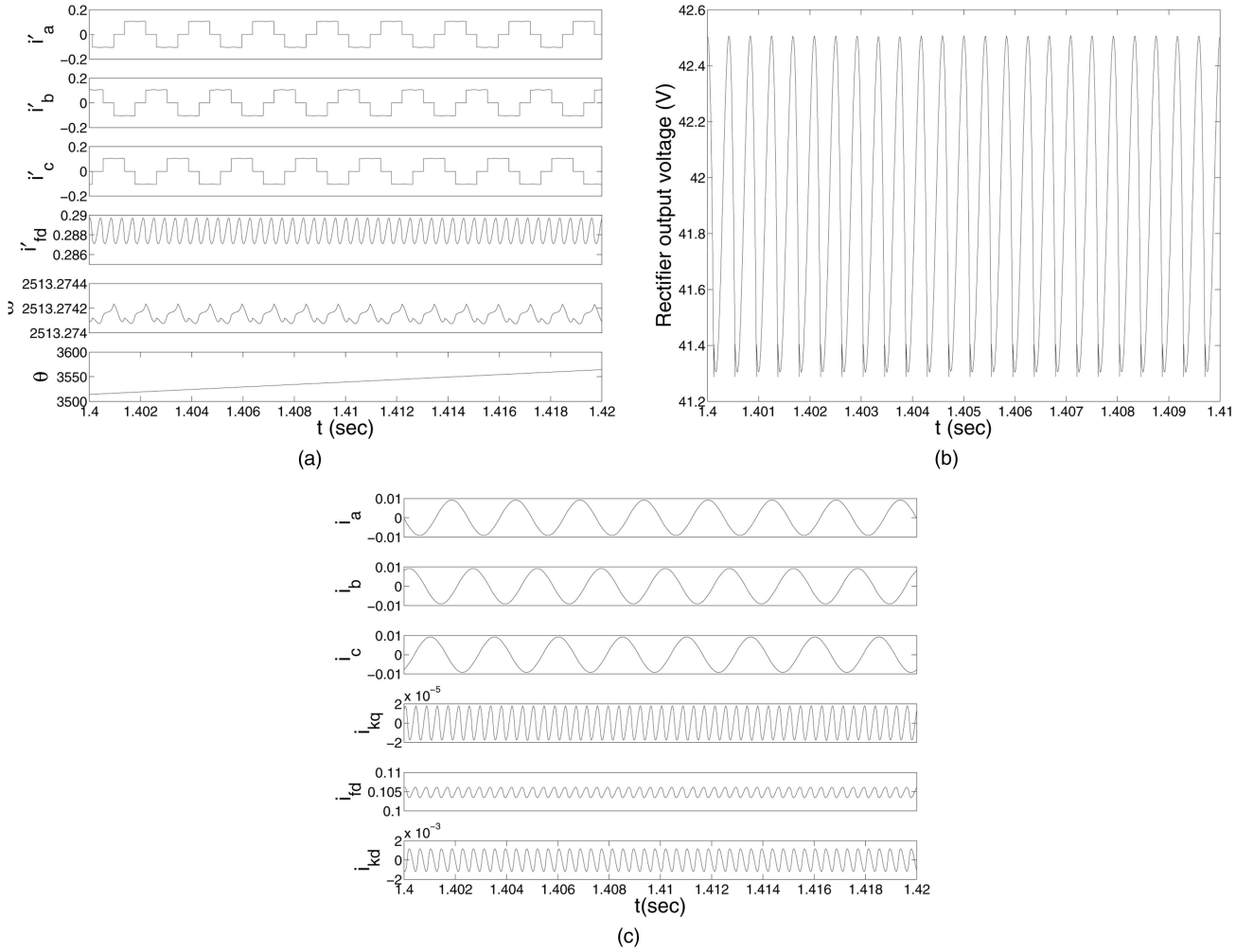

Fig. 7. Nominal behavior for brushless generator. (a) Exciter generator currents, angular velocity, and angular displacement. Phase currents take turns to switch on and off, field current has small magnitude oscillations around its steady state value. Angular velocity has very small perturbations due to the PI controller dynamic behavior. (b) Rectifier output voltage is typical output from 3-phase diode rectifier, where sinusoidal ripples are superimposed on average dc voltage. (c) Main generator winding currents. 3-phase currents are sinusoidal signals with $\pi/3$ phase shifts; damper winding currents are effectively zero with very small magnitude oscillations, and field winding current has same sinusoidal ripples of rectifier output voltage, with much smaller magnitude.

then both signals have oscillations with sufficient magnitude that could be exploited for fault detection. Furthermore, the oscillations are out of phase by π deg rad.

2) *Dual Diode Fault*: The system is simulated with an open circuit fault in diodes D_{aT} and D_{bB}, injected at time $t = 0.5$ s, which results in the discrete mode set $\{BC, BA, CA, OFF\}$, and the automaton in Fig. 6(a). The following signals are observed (Fig. 9).

Exciter generator winding currents: because of the excluded modes, $\hat{i}_a \leq 0$ and $\hat{i}_b \geq 0$. The exciter field current undergoes periodic oscillations with very similar waveform to the rectifier output voltage.

Rectifier output voltage: the voltage goes to zero for the duration of mode *AB* (1/6 the output voltage period ≈ 0.42 ms), as explained in Section VI. The discrepancy with Fig. 6(b) is due to the fact that the 3-phase output from the exciter generator is not pure sinusoidal with rectifier diode faults. The negative spike is an artifact of hybrid systems simulation when switching modes, and is not part of the system dynamics.

Main generator winding currents: slight distortion is noted in phases *abc* output currents, but not with a sufficient magnitude to allow robust fault detection. The field winding signal behavior is very similar to the output voltage. The behavior for damper winding currents is the same as in the case of a single diode fault, namely out of phase spikes, followed by large magnitude periodic oscillations.

It can be shown that other diode faults have similar effects, except for phase differences. As a conclusion, fault signatures for different diode faults are very similar with regard to main generator damper winding and phase currents. The distinguishing signals are the exciter phase winding currents, the main generator field winding current, and the rectifier output voltage. These facts are illustrated by Table V, which

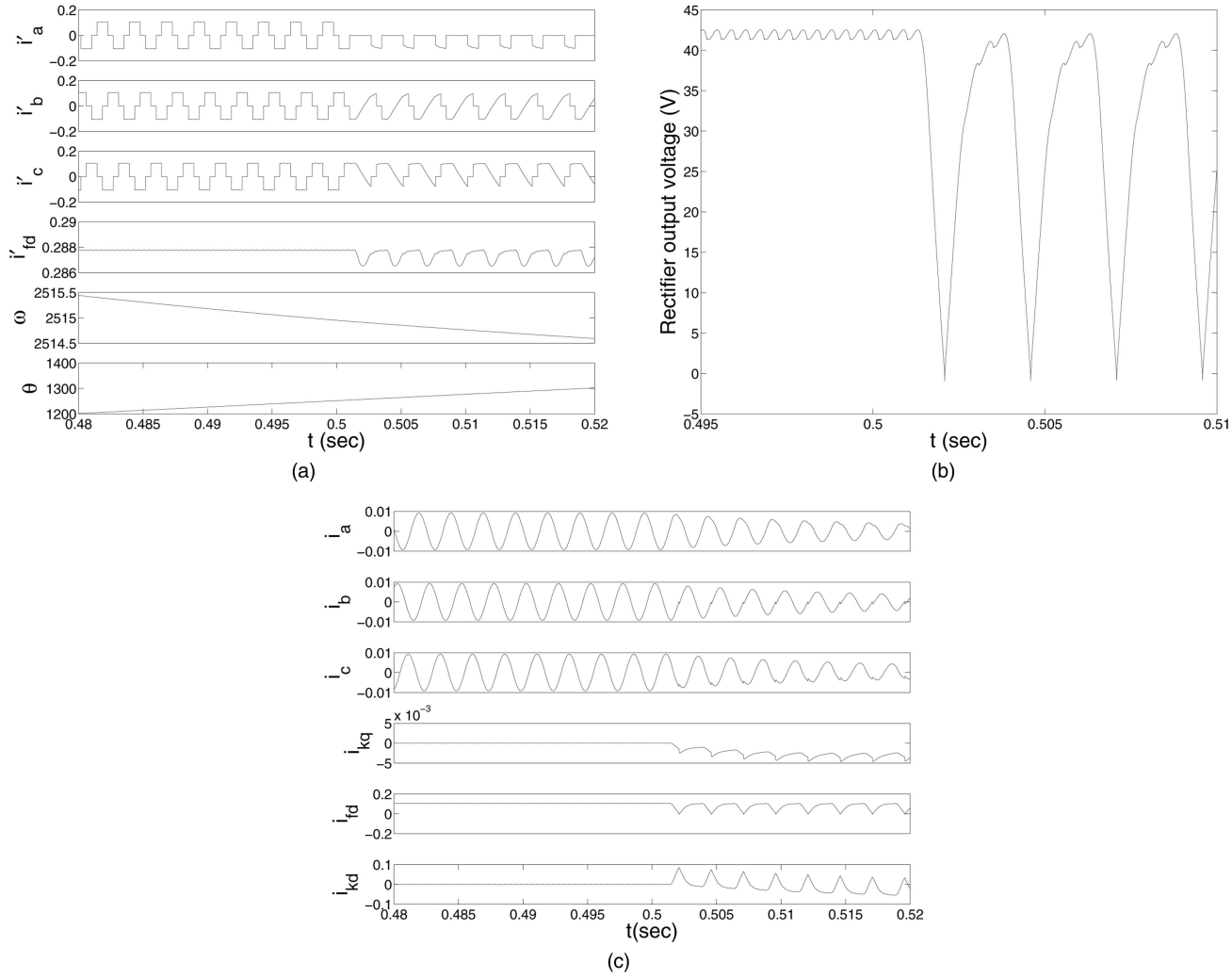

Fig. 8. Behavior of brushless generator with single diode fault, diode D_{aT} in Fig. 2 fails open. (a) Exciter generator currents, angular velocity, and angular displacement. Phase current $\hat{i}_a \leq 0$ and $\hat{i}_b$ and $\hat{i}_c$ do not transition abruptly from negative to positive and vice versa, respectively. Field current $\hat{i}_{fd}$ has periodic oscillations with same waveform as rectifier output voltage. No noticeable effect on angular velocity. (b) Rectifier output voltage returns to zero due to excluded modes *AB* and *AC* resulting from diode fault. (c) Main generator winding currents. 3-phase currents are slightly distorted. Damper winding currents i_{kq} and i_{kd} have negative and positive spikes, respectively, at fault injection time, and then undergo periodic oscillations with high magnitude compared with their steady state zero value.

summarizes the system behavior with nominal and different fault types. It represents the fault signature table that could be further exploited to develop fault detection algorithms for different types of faults.

C. Parametric Faults Injection

We consider an abrupt change in the resistance of the field winding of the main generator r_{fd}. In practice this may be caused by winding overheating. A 10% sudden increase in the resistance value is injected at simulation time $t = 0.5$ s, and the following signals are observed (Fig. 10).

Exciter generator winding currents: the only notable behavior is the transient reduction in current magnitude, while no effect is noted on the angular velocity.

Rectifier output voltage: a reduction in the rectifier output voltage is noted, due to the higher input impedance of the main generator field winding. The spike at the time of fault injection is an artifact due to the switching behavior of the hybrid system, and is not part of the system dynamics.

Main generator winding currents: the phase currents undergo sudden decrease of the magnitude. The most notable fault signature is in the damper winding *kq* current signal, that shows a negative spike and damped oscillations. A very similar behavior is noted for damper winding *kd* current, but with positive spike.

We conclude that for parametric abrupt faults, only magnitude change is noted, and as long as the fault magnitude is within the control range of the GCU, the GCU will compensate the 3-phase output signal

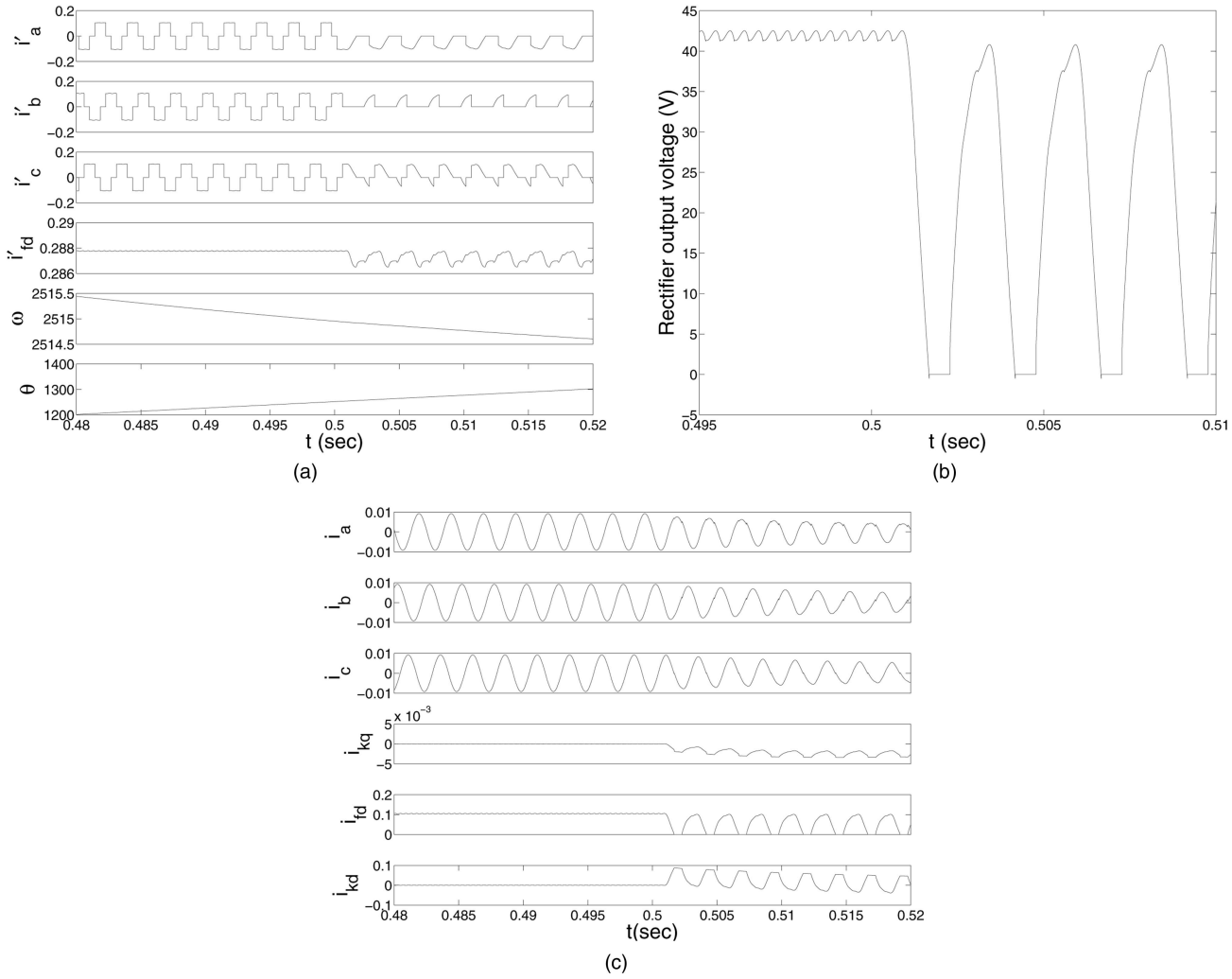

Fig. 9. Behavior of brushless generator with dual diode fault, diodes D_{aT} and D_{bB} in Fig. 2 fail open. (a) Exciter generator currents, angular velocity, and angular displacement. Phase current $\hat{i}_a \leq 0$ and $\hat{i}_b \geq 0$. Field current $\hat{i}_{fd}$ undergoes oscillations with waveform very similar to rectifier output voltage. No noticeable effect on angular velocity. (b) Rectifier output voltage returns to zero for the duration of mode AB. (c) Main generator winding currents. 3-phase currents are slightly distorted. Damper winding currents i_{kq} and i_{kd} have negative and positive spikes, respectively, at the fault injection time, and then undergo periodic oscillations with high magnitude compared with their steady state zero values.

for the fault effect. Therefore, detection of the fault using the 3-phase output signal may be hard if the response time of the GCU is small. On the other hand monitoring phase currents for the exciter generator and damper winding currents is likely to be more effective for detecting this kind of faults, provided they are measurable or could be estimated using a system observer (see discussion in Section VIII). Table V summarizes the resistance fault signatures.

Table V summarizes the system behavior with nominal and different fault types discussed in this section. It represents the fault signature table that could be further exploited to develop fault detection algorithms for different types of faults.

VIII. DISCUSSION OF MODELING AND SIMULATION RESULTS

The results of the simulation experiments show that fault signatures are mostly notable in the current signals of the rotating windings, namely phase windings of the exciter generator and field/damper windings of the main generator. Fault signature in output phase currents is not easily detectable, especially that phase currents have much higher frequency. Therefore, to detect faults from these waveforms, either faster sensors are required or frequency response analysis is needed. However, and as pointed out before, most of the existing techniques for generator fault detection rely on phase current measurements and harmonic analysis, making it harder to discriminate between faults. Given these facts, internal winding currents of the exciter and main generators represent potential candidates for detecting diode and parametric faults.

In most practical installations, internal winding current measurements are not directly measurable, since these windings are mounted on the rotating part of the generator, making it unusually hard to

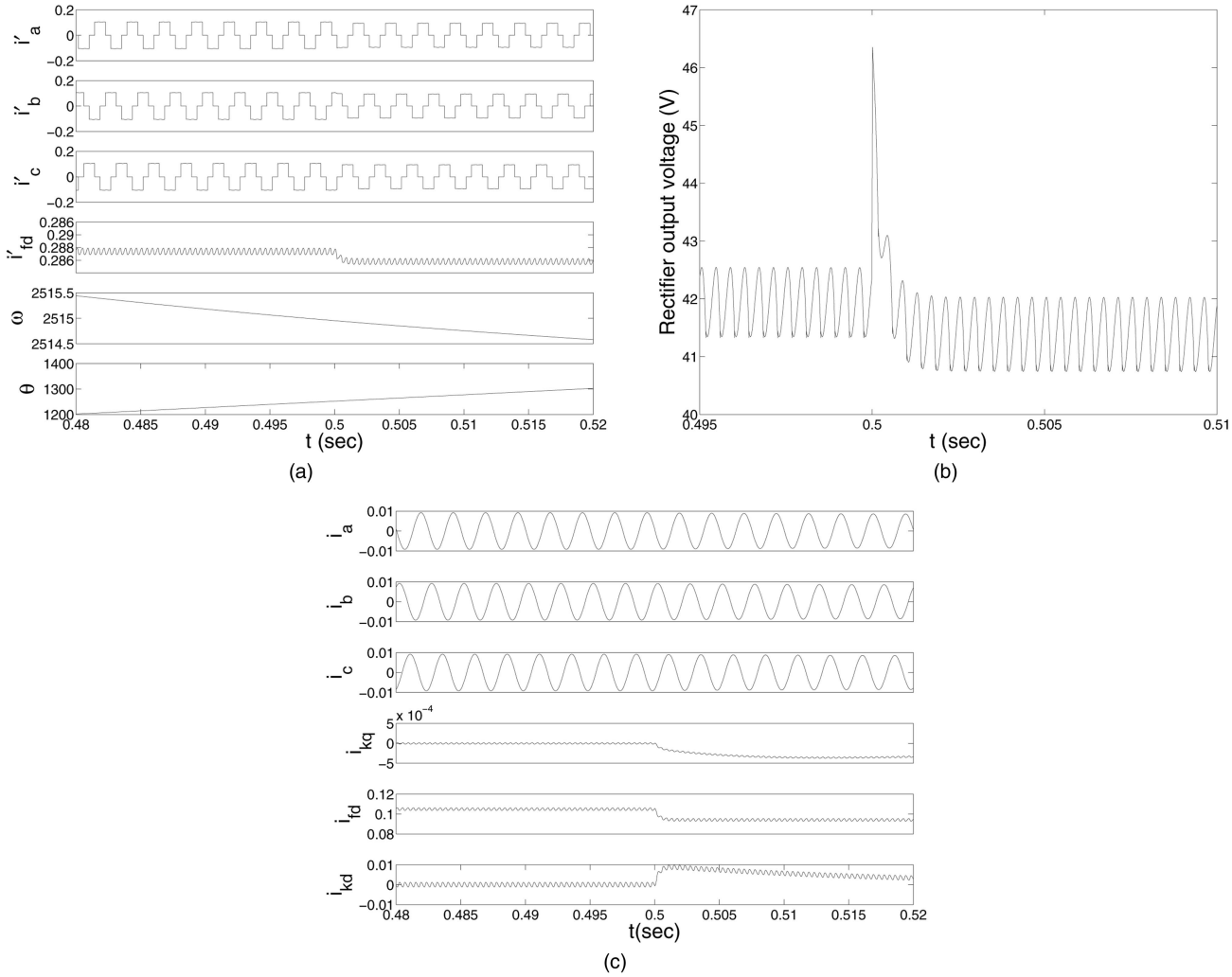

Fig. 10. Behavior of brushless generator with abrupt parametric fault in main generator field winding resistance r_{fd}. (a) Exciter generator currents, angular velocity, and angular displacement. Transient reduction of current magnitude occurs. No impact on angular velocity is noted. (b) Rectifier output voltage decreases due to higher input impedance of field winding. (c) Main generator winding currents. Transient decrease in 3-phase currents is noted. Damper winding currents i_{kq} and i_{kd} show negative and positive spikes, followed by small oscillations and return to zero.

install sensors that produce reliable measurements. One way to solve this problem is to estimate the unmeasurable currents using the brushless generator state-space model. Some work on the use of observers for damper winding currents to estimate generator parameters has been reported in [16]. However, the authors are not aware of any work that addresses the observer design for the complete brushless generator, which has to be a hybrid observer. The starting point is to use the model presented in Section IV, perhaps with some relaxing assumptions to simplify the hybrid observer design. One such practical assumption is that the angular velocity of the machine is constant during normal and faulty behavior of the machine operation. The results of our simulation experiment presented in this paper, in addition to the feedback obtained from our industrial partners, have shown very small effect of the faults considered on the variability of the angular velocity. This assumption has the effect of transforming the system into a linear, but a time-varying (LTV) system, thereby making the observer design much simpler.

The brushless generator hybrid model developed in this paper can be used for FDI by augmenting it with a bank of hybrid observers; one observer for the nominal system model, and an additional observer with the faulty system model for each fault to be detected. The hybrid observer has, as its input, the brushless generator input $u = [V_F \;\; T_m]$ and output $y = [i_a \;\; i_b \;\; i_c]$, and is composed of a location observer and a continuous observer. The location observer estimates the current system mode $\hat{q}$, and the continuous observer estimates the continuous system states $\hat{\mathbf{x}}$, given the current system mode from the location observer [13]. Detection of faults presented in this paper is accomplished by comparing the estimated states $\hat{\mathbf{x}}$ from the hybrid observer with the

TABLE V
Brushless Generator Fault Signatures

Fault	$\hat{i}_a$	$\hat{i}_b$	$\hat{i}_f$	v_{rec}	$i_a \backslash i_b \backslash i_c$	i_{kq}	i_{kd}
Nominal		⌞ 0.83 ms ⌜	DC	3-ph rectified	3-ph sin.	0	0
Single diode fault	≤ 0	⌞ 2.5 ms ⌞	$\downarrow,\sim$	hits zero every 2.5 ms	$\downarrow -$	$\downarrow,\sim$	$\uparrow,\sim$
Dual diode fault	≤ 0	≥ 0	$\downarrow,\sim$	⌞ 2.5 ms ⌞	$\Downarrow -$	$\downarrow,\sim$	$\uparrow,\sim$
Resistance fault	$\downarrow\uparrow$	$\downarrow\uparrow$	$\downarrow\uparrow$	$\downarrow\uparrow$	$\downarrow -$	$\downarrow -$	$\uparrow -$

Note:
$\uparrow$ signal magnitude increase
$\Uparrow$ signal magnitude increase (qualitatively higher than $\uparrow$)
$\downarrow$ signal magnitude decrease
$\Downarrow$ signal magnitude decrease (qualitatively lower than $\downarrow$)
$-$ signal nominal value
$\sim$ signal oscillations around its nominal value
⌞ signal returns to zero from positive magnitude, remains zero for 0.42 ms
⌜ signal returns to zero from negative magnitude, remains zero for 0.42 ms
$\uparrow\downarrow$ signal magnitude increase, followed by a signal magnitude decrease
⌞ T ⌞ signal returns to zero from positive magnitude every T ms, remains zero for 0.42 ms

least residual to the signals in Table V to discriminate between faults.

Some comments about the brushless generator model presented in this paper are in order. The model assumes linear magnetic circuits, where there is no saturation in the machine. Most modern generating systems are designed to work in the linear region of the magnetic curve, therefore, this should not be a limiting factor in using the model. However, if the objective is to simulate the machine with overload conditions, or if the fault to be simulated drives the machine into the saturation region, then the model has to be extended to include saturation effect. Also, in some practical designs, a filter capacitor is added to the output of the rectifier circuit to smooth the output voltage that is applied to the main field winding. This capacitor will try to maintain the rectifier output voltage during diode failure, so that the voltage does not return to zero, unlike the simulation results in this paper. However, the analysis will be similar with the addition of one state variable representing the capacitor voltage.

Finally, as an extension to this study, the model could be evaluated using a laboratory setup akin to the one presented in [19], where different diode faults could be injected. The model implemented in Matlab/Simulink could be simulated offline or in real-time on a personal computer to compare the results. Further, laboratory measurements could be communicated to the model for further analysis and tuning, using Matlab Instrument Control Toolbox and the appropriate input/output digital interface.

IX. CONCLUSIONS

In this paper, we have presented a hybrid modeling approach for brushless generators with nominal and faulty conditions. Direct phase-domain (abc domain) modeling is shown to facilitate generator modeling, especially with machine faults, since it avoids unnecessary transformations introduced by the dq modeling approach. The hybrid modeling approach presented is an accurate method to model brushless generators with faults in the exciter generator/rectifier parts. It has been shown also that with diode faults, the hybrid modeling approach helps in understanding the physics of failure events, by defining a framework for modeling and simulation of different combinations of faults.

For different rotor faults, the fault signatures generated have shown that currents in the rotating windings are more appropriate for FDI. On the other hand, the 3-phase output currents as well as the excitation current do not show fault signatures different from what has been reported in the literature about other types of machine faults.

As a future work, we are investigating the use of the hybrid model in building accurate FDI schemes for the different faults discussed in the paper. The use of a hybrid observer along with the fault signatures developed is to be investigated, and the power of the FDI scheme is to be compared with existing techniques for brushless generator fault detection.

ACKNOWLEDGMENT

The authors would like to thank Hamilton Sundstrand Corporation, for their guidance during this work.

APPENDIX

The expressions for the inductance matrices of the main and exciter generators, and their derivatives, are given by (21)–(24).

$$\mathbf{L}=\begin{bmatrix}
-L_{ls}-L_A+L_B\cos(2\theta_r) & \frac{L_A}{2}+L_B\cos\left(2\theta_r-\frac{2\pi}{3}\right) & \frac{L_A}{2}+L_B\cos\left(2\theta_r+\frac{2\pi}{3}\right) & L_{skq}\cos\theta_r & L_{sfd}\sin\theta_r & L_{skd}\sin\theta_r \\
\frac{L_A}{2}+L_B\cos\left(2\theta_r-\frac{2\pi}{3}\right) & -L_{ls}-L_A+L_B\cos\left(2\theta_r-\frac{4\pi}{3}\right) & \frac{L_A}{2}+L_B\cos(2\theta_r) & L_{skq}\cos\left(\theta_r-\frac{2\pi}{3}\right) & L_{sfd}\sin\left(\theta_r-\frac{2\pi}{3}\right) & L_{skd}\sin\left(\theta_r-\frac{2\pi}{3}\right) \\
\frac{L_A}{2}+L_B\cos\left(2\theta_r+\frac{2\pi}{3}\right) & \frac{L_A}{2}+L_B\cos(2\theta_r) & -L_{ls}-L_A+L_B\cos\left(2\theta_r+\frac{4\pi}{3}\right) & L_{skq}\cos\left(\theta_r+\frac{2\pi}{3}\right) & L_{sfd}\sin\left(\theta_r+\frac{2\pi}{3}\right) & L_{skd}\sin\left(\theta_r+\frac{2\pi}{3}\right) \\
-L_{skq}\cos\theta_r & -L_{skq}\cos\left(\theta_r-\frac{2\pi}{3}\right) & -L_{skq}\cos\left(\theta_r+\frac{2\pi}{3}\right) & L_{lkq}+L_{mkq} & 0 & 0 \\
-L_{sfd}\sin\theta_r & -L_{sfd}\sin\left(\theta_r-\frac{2\pi}{3}\right) & -L_{sfd}\sin\left(\theta_r+\frac{2\pi}{3}\right) & 0 & L_{lfd}+L_{mfd} & L_{fdkd} \\
-L_{skd}\sin\theta_r & -L_{skd}\sin\left(\theta_r-\frac{2\pi}{3}\right) & -L_{skd}\sin\left(\theta_r+\frac{2\pi}{3}\right) & 0 & L_{fdkd} & L_{lkd}+L_{mkd}
\end{bmatrix} \tag{21}$$

$$\dot{\mathbf{L}}=\begin{bmatrix}
-2L_B\sin(2\theta_r) & -2L_B\sin\left(2\theta_r-\frac{2\pi}{3}\right) & -2L_B\sin\left(2\theta_r+\frac{2\pi}{3}\right) & -L_{skq}\sin\theta_r & L_{sfd}\cos\theta_r & L_{skd}\cos\theta_r \\
-2L_B\sin\left(2\theta_r-\frac{2\pi}{3}\right) & -2L_B\sin\left(2\theta_r-\frac{4\pi}{3}\right) & -L_B\sin(2\theta_r) & -L_{skq}\sin\left(\theta_r-\frac{2\pi}{3}\right) & L_{sfd}\cos\left(\theta_r-\frac{2\pi}{3}\right) & L_{skd}\cos\left(\theta_r-\frac{2\pi}{3}\right) \\
-2L_B\sin\left(2\theta_r+\frac{2\pi}{3}\right) & -2L_B\sin(2\theta_r) & -2L_B\sin\left(2\theta_r+\frac{4\pi}{3}\right) & -L_{skq}\sin\left(\theta_r+\frac{2\pi}{3}\right) & L_{sfd}\cos\left(\theta_r+\frac{2\pi}{3}\right) & L_{skd}\cos\left(\theta_r+\frac{2\pi}{3}\right) \\
L_{skq}\sin\theta_r & L_{skq}\sin\left(\theta_r-\frac{2\pi}{3}\right) & L_{skq}\sin\left(\theta_r+\frac{2\pi}{3}\right) & 0 & 0 & 0 \\
-L_{sfd}\cos\theta_r & -L_{sfd}\cos\left(\theta_r-\frac{2\pi}{3}\right) & -L_{sfd}\cos\left(\theta_r+\frac{2\pi}{3}\right) & 0 & 0 & 0 \\
-L_{skd}\cos\theta_r & -L_{skd}\cos\left(\theta_r-\frac{2\pi}{3}\right) & -L_{skd}\cos\left(\theta_r+\frac{2\pi}{3}\right) & 0 & 0 & 0
\end{bmatrix}\omega \tag{22}$$

$$\hat{\mathbf{L}}=\begin{bmatrix}
-\hat{L}_{ls}-\hat{L}_A+\hat{L}_B\cos(2\theta_r) & \frac{\hat{L}_A}{2}+\hat{L}_B\cos\left(2\theta_r-\frac{2\pi}{3}\right) & \frac{\hat{L}_A}{2}+\hat{L}_B\cos\left(2\theta_r+\frac{2\pi}{3}\right) & \hat{L}_{sfd}\sin\theta_r \\
\frac{\hat{L}_A}{2}+\hat{L}_B\cos\left(2\theta_r-\frac{2\pi}{3}\right) & -\hat{L}_{ls}-\hat{L}_A+\hat{L}_B\cos\left(2\theta_r-\frac{4\pi}{3}\right) & \frac{\hat{L}_A}{2}+\hat{L}_B\cos(2\theta_r) & \hat{L}_{sfd}\sin\left(\theta_r-\frac{2\pi}{3}\right) \\
\frac{\hat{L}_A}{2}+\hat{L}_B\cos\left(2\theta_r+\frac{2\pi}{3}\right) & \frac{\hat{L}_A}{2}+\hat{L}_B\cos(2\theta_r) & -\hat{L}_{ls}-\hat{L}_A+\hat{L}_B\cos\left(2\theta_r+\frac{4\pi}{3}\right) & \hat{L}_{sfd}\sin\left(\theta_r+\frac{2\pi}{3}\right) \\
-\hat{L}_{sfd}\sin\theta_r & -\hat{L}_{sfd}\sin\left(\theta_r-\frac{2\pi}{3}\right) & -\hat{L}_{sfd}\sin\left(\theta_r+\frac{2\pi}{3}\right) & \hat{L}_{lfd}+\hat{L}_{mfd}
\end{bmatrix} \tag{23}$$

$$\dot{\hat{\mathbf{L}}}=\begin{bmatrix}
-2\hat{L}_B\sin(2\theta_r) & -2\hat{L}_B\sin\left(2\theta_r-\frac{2\pi}{3}\right) & -2\hat{L}_B\sin\left(2\theta_r+\frac{2\pi}{3}\right) & \hat{L}_{sfd}\cos\theta_r \\
-2\hat{L}_B\sin\left(2\theta_r-\frac{2\pi}{3}\right) & -2\hat{L}_B\sin\left(2\theta_r-\frac{4\pi}{3}\right) & -2\hat{L}_B\sin(2\theta_r) & \hat{L}_{sfd}\cos\left(\theta_r-\frac{2\pi}{3}\right) \\
-2\hat{L}_B\sin\left(2\theta_r+\frac{2\pi}{3}\right) & -2\hat{L}_B\sin(2\theta_r) & -2\hat{L}_B\sin\left(2\theta_r+\frac{4\pi}{3}\right) & \hat{L}_{sfd}\cos\left(\theta_r+\frac{2\pi}{3}\right) \\
-\hat{L}_{sfd}\cos\theta_r & -\hat{L}_{sfd}\cos\left(\theta_r-\frac{2\pi}{3}\right) & -\hat{L}_{sfd}\cos\left(\theta_r+\frac{2\pi}{3}\right) & 0
\end{bmatrix}\omega. \tag{24}$$

REFERENCES

[1] Anderson, P. M. and Fouad, A. A.
Power System Control and Stability.
Piscataway, NJ: IEEE Press Power Engineering Series, 2005.

[2] Antsaklis, P. J. and Koutsoukos, X. D.
Hybrid systems: Review and recent progress.
In *Software-Enabled Control: Information Technology for Dynamical Systems*, Hoboken, NJ: Wiley-IEEE Press, 2003.

[3] Batard, C., Poitiers, F., and Machmoum, M.
An original method to simulate diodes rectifiers behaviour with Matlab-Simulink taking into account overlap phenomenon.
In *Proceedings of the IEEE International Symposium on Industrial Electronics* (ISIE 2007), June 2007, 971–976.

[4] Batzel, T. and Swanson, D.
Prognostic health management of aircraft power generators.
IEEE Transactions on Aerospace and Electronic Systems, **45**, 2 (Apr. 2009), 473–482.

[5] Bo, Z., et al.
Non-differential protection of a generator's stator utilizing fault transients.
In *Proceedings of the IEE Seventh International Conference on Developments in Power System Protection*, 2001, 503–506.

[6] Bo, Z., et al.
Non-differential protection of generator using fuzzy neural network.
In *Proceedings of the International Conference on Power System Technology* (POWERCON '98), vol. 2, Aug. 1998, 1072–1076.

[7] Breingan, W., et al.
Survey of experience with generator protection and prospects for improvements using digital computers.
IEEE Transactions on Power Delivery, **3**, 4 (1988), 1511–1522.

[8] Connally, H. M., et al.
Detection of interturn faults in generator rotor windings using airgap search coil.
IEE Conference Publication, vol. 254, 1985, 11–15.

[9] Duda, R. O., Hart, P. E., and Stork, D. G.
Pattern Classification.
Hoboken, NJ: Wiley-Interscience, 2000.

[10] Frank, P. M.
Fault diagnosis in dynamic systems using analytical and knowledge-based redundancy—A survey and some new results.
Automatica, **26** (1990), 459–474.

[11] Gertler, J. J.
Fault Detection and Diagnosis in Engineering Systems.
New York: Marcel Dekker, 1998.

[12] Isermann, R.
Model-based fault-detection and diagnosis—Status and applications.
Annual Reviews in Control, **29** (2005), 71–85.

[13] Koutsoukos, X., Kurien, J., and Zhao, F.
Estimation of distributed hybrid systems using particle filtering methods.
In *Hybrid Systems: Computation and Control*, vol. 2623/2003, Berlin: Springer, 2003, 298–313.

[14] Krause, P. C., Wasynczuk, O., and Sudhoff, S. D.
Analysis of Electric Machinery and Drive Systems.
Piscataway, NJ: IEEE Press Power Engineering Series, 2002.

[15] Kulkarni, A., et al.
Development of a technique for on-line detection of shorts in field windings of turbine-generator rotors: Circuit design and testing.
IEEE Transactions on Energy Conversion, **15**, 1 (Mar. 2000), 8–13.

[16] Kyriakides, E., Heydt, G., and Vittal, V.
On-line estimation of synchronous generator parameters using a damper current observer and a graphic user interface.
IEEE Transactions on Energy Conversion, **19**, 3 (Sept. 2004), 499–507.

[17] Li, X-Y.
A microprocessor-based fault monitor for rotating rectifiers of brushless ac exciters using a pattern-recognition approach.
In *Proceedings of the IEEE Instrumentation and Measurement Technology Conference* (IMTC/94), vol. 1, May 1994, 394–397.

[18] The MathWorks, Inc.
Simulink 7 Using Simulink.
The MathWorks, Inc., Natick, MA, Mar. 2008.

[19] McArdle, M. and Morrow, D.
Noninvasive detection of brushless exciter rotating diode failure.
IEEE Transactions on Energy Conversion, **19**, 2 (June 2004), 378–383.

[20] Megahed, A. and Malik, O.
An artificial neural network based digital differential protection scheme for synchronous generator stator winding protection.
IEEE Transactions on Power Delivery, **14**, 1 (Jan. 1999), 86–93.

[21] Megahed, A. and Malik, O.
Synchronous generator internal fault computation and experimental verification.
IEE Proceedings—Generation, Transmission and Distribution, **145**, 5 (Sept. 1998), 604–610.

[22] Mouni, E., Tnani, S., and Champenois, G.
Comparative study of three modelling methods of synchronous generator.
In *Proceedings of the IEEE 32nd Annual Conference on Industrial Electronics*, Nov. 2006, 1551–1556.

[23] Narasimhan, S., Mosterman, P. J., and Biswas, G.
A systematic analysis of measurement selection algorithms for fault isolation in dynamic systems.
In *Proceedings of the International Workshop on Diagnosis Principles*, Cape Cod, MA, 1998, 94–101.

[24] Park, R. H.
Two-reaction
theory of synchronous machines—Generalized method of analysis, Part I and II.
Transactions of the American Institute of Electrical Engineers, **48**, 3 (July 1929), 716–727.

[25] Penman, J. and Jiang, H.
The detection of stator and rotor winding short circuits in synchronous generators by analyzing excitation current harmonics.
In *Proceedings of the International Conference on Opportunities and Advances in International Electric Power Generation*, Mar. 1996, 137–142.

[26] Senesky, M., Eirea, G., and Koo, T. J.
Hybrid modeling and control of power electronics.
In *Hybrid Systems: Computation and Control, Lecture Notes in Computer Science Series*, vol. 2623/2003, Berlin: Springer, 2003, 450–465.

[27] Sottile, J., Trutt, F., and Leedy, A.
Condition monitoring of brushless three-phase synchronous generators with stator winding or rotor circuit deterioration.
IEEE Transactions on Industry Applications, **42**, 5 (Sept.–Oct. 2006), 1209–1215.

[28] Srivastava, K. and Berggren, B.
Simulation of synchronous machines in phase coordinates including magnetic saturation.
Electric Power Systems Research, **56** (2000), 177–183.

[29] Tantawy, A., Koutsoukos, X., and Biswas, G.
Aircraft AC generators: Hybrid system modeling and simulation.
Presented at the International Conference on Prognostics and Health Management (PHM08), 2008.

Ashraf Tantawy received his B.Sc. in electronics and communication engineering from Ain Shams University, Cairo, Egypt, in 1995. He received a Master of Science in computer science from the University of Louisville, KY, in 2005, and a Master of Science and a Ph.D. in electrical engineering from Vanderbilt University, Nashville, TN, in 2008 and 2011, respectively.

From 1995 to 2005, he was a telecommunication and control systems engineer working in the design and implementation of communication and control systems for the oil and gas industry. Since 2007, he has been a graduate research assistant with the Institute for Software Integrated Systems, Department of Electrical Engineering and Computer Science, Vanderbilt University. His research interests include statistical signal processing, wireless communications, sensor networks, embedded systems, and modeling and simulation of complex hybrid systems.

Xenofon Koutsoukos received his Diploma in electrical and computer engineering from the National Technical University of Athens (NTUA), Greece in 1993. He received the Master of Science in electrical engineering in January 1998 and the Master of Science in applied mathematics in May 1998 both from the University of Notre Dame. He received his Ph.D. in electrical engineering working under Professor Panos J. Antsaklis with the group for Interdisciplinary Studies of Intelligent Systems.

He is an associate professor in the Department of Electrical Engineering and Computer Science at Vanderbilt University. He is also a senior research scientist in the Institute for Software Integrated Systems (ISIS). Before joining Vanderbilt, he was a member of research staff in the Xerox Palo Alto Research Center (PARC) (2000–2002), working in the Embedded Collaborative Computing Area. Between 1993 and 1995, he joined the National Center for Space Applications, Hellenic Ministry of National Defense, Athens, Greece as a computer engineer in the areas of image processing and remote sensing. His research work is in the area of cyber-physical systems with emphasis on formal methods, distributed algorithms, diagnosis and fault tolerance, and adaptive resource management.

Dr. Koutsoukos has published numerous journal and conference papers and he is co-inventor of four U.S. patents. He was the recipient of the NSF Career Award in 2004 and the Excellence in Teaching Award in 2009 from the Vanderbilt University School of Engineering.

Gautam Biswas has an undergraduate degree in electrical engineering from the Indian Institute of Technology (IIT) in Mumbai, India, and M.S. and Ph.D. degrees in computer science from Michigan State University, East Lansing, MI.

He is a Professor of Computer Science and Computer Engineering in the EECS Department and a Senior Research Scientist at the Institute for Software Integrated Systems (ISIS) at Vanderbilt University. He conducts research in intelligent systems with primary interests in hybrid modeling, simulation, and analysis of complex embedded systems, and their applications to diagnosis, prognosis, and fault-adaptive control. As part of this work, he has worked on fault-adaptive control of fuel transfer systems for aircraft, and Advanced Life Support systems for NASA. He has also initiated new projects in health management of complex systems. More recently, he is working on combining model-based and data-driven approaches for diagnostic and prognostic reasoning. A second area of research is in planning and scheduling of tasks in complex, distributed applications, such as a sensor web. In other research projects, he is involved in developing simulation-based environments for learning and instruction.

Dr. Biswas has published extensively, and has over 300 refereed publications. He is an Associate Editor of the *IEEE Transactions on Systems, Man, and Cybernetics*, *Prognostics and Health Management*, and *Educational Technology and Society Journal*. He has served on the program committee of a number of conferences, and most recently was Program Cochair of the 18th International Workshop on Principles of Diagnosis. He is currently serving on the executive committee of the Asia Pacific Society for Computers in Education. He is a Senior Member of the IEEE Computer Society, ACM, AAAI, and the Sigma Xi Research Society.